CONEM 2016 CONGRESSO NACIONAL DE ENGENHARIA MECÂNICA
21 - 25 AGOSTO DE 2016 FORTALEZA - CEARÁ
ABCM 40 anos Associação Brasileira de Engenharia e Ciências Mecânicas

VERTICAL DYNAMICS OF A FULLY INDEPENDENT SUSPENSION VEHICLE

Rodrigo Veronese Moreira, rodrigo_vr@msn.com [1,2]
Alberto Paiva, paiva.ufrj@gmail.com [1]

[1] Universidade Federal Fluminense
Volta Redonda School of Engineering
Department of Mechanical Engineering
420 Trabalhadores Av. – Volta Redonda – RJ – Brazil – 27.255-250

[2] Semcon do Brasil
Tests Engineering Department
8005 Renato Monteiro St.
Porto Real – RJ – Brazil – 27.570-000

Resumo: *Vehicle dynamics has been a point of great interest since the very beginning, when vehicles started to evolve in the early 1900's. Since then, a lot of physical models have been proposed – from the simple quarter-car model up to all-inclusive vehicle models. Moreover, localized refinement of these models may be introduced to scrutinize some desired features. With no doubts, commercial packages play an outstanding role to simulate more elaborated models. Nevertheless, handmade-implemented numerical codes enable thorough dynamical analyses. This paper presents a complete vehicle model, where the physical archetype consists of a seven-degree of freedom (**DOF**) system; where three of them are associated with the bounce, pitch and roll displacements of the vehicle chassis, while the four remaining **DOF**'s are related to the independent suspension unsprung masses. To solve the resulting set of ordinary differential equations, the fourth-order Runge-Kutta method is employed. The parameters adopted in the simulations are related to a 4x2 commercial light truck, including empirical nonlinear performance curves for the front and rear suspension stiffness and damping, provided by a specific manufacturer. The numerical results consider three different pavement conditions - namely: a cobblestone road; a speed bump and a hole on the road. Besides, changes in the dynamical response are investigated through comparisons regarding: loaded/unloaded truck configurations and linear/nonlinear suspension elements (spring and damper), as well as variations in the performance curves for these elements.*

Keywords: *Vehicle dynamics, fully independent suspension, nonlinear stiffness and damping.*

1. INTRODUCTION

Modeling vehicle dynamics is not a trivial task. Many efforts have been done towards a complete vehicle modeling; however, most of them make use of either simple models with localized refinements or commercial packages, in order to conceive an all-inclusive model. Within this context, it is possible to highlight some works dealing with quarter-car models, such as: Türkay & Akçay (2005); Litak *et al*. (2008); Taffo & Siewea (2013) and some papers concerning half-car models, such as: Vallurupalli *et al*. (1995); Rao & Narayanan (2008). Concerning full-car articles, Dugard *et al*. (2012) and Sharma *et al*. (2016) are some recent contributions, among others. The present paper focuses on the dynamical modeling and numerical simulation of a 4x2 commercial light truck model, considering real nonlinear performance curves for the front and rear suspension stiffness and damping. The resulting equations are implemented in a handmade open code, using the fourth-order *Runge-Kutta* method. Numerical results take into account comparisons involving: different pavement conditions; nonlinear behavior of the suspension elements and load addition implications.

2. DYNAMICAL MODELING

This section includes the dynamical physical model and its respective mathematical formulation. The resulting equations of motion are obtained using the *Newton-Euler* formalism.

Figure 1 presents the physical sketch with seven degrees of freedom (**DOF**), representing a 4x2 commercial light truck. It consists of a rigid platform that represents the vehicle chassis and four unsprung masses related to the independent suspension elements on its four wheels. The platform encompasses three **DOF**'s associated with bounce, pitch and roll displacements. Concerning the four unsprung masses, each of them has only one **DOF** related to its respective absolute linear displacement in the "z" direction, resulting in a total number of four **DOF**'s. The chassis is connected to each suspension unsprung mass through a spring-dashpot assembly in parallel, representing the suspension stiffness and damping, respectively; which, in turn, is connected to the ground through another spring-dashpot assembly in parallel, representing the tires behavior. For more details about vehicle dynamics modeling, please refer to the following literature: Gillespie (1992); Wong (2001) and Nicolazzi *et al*. (2001).

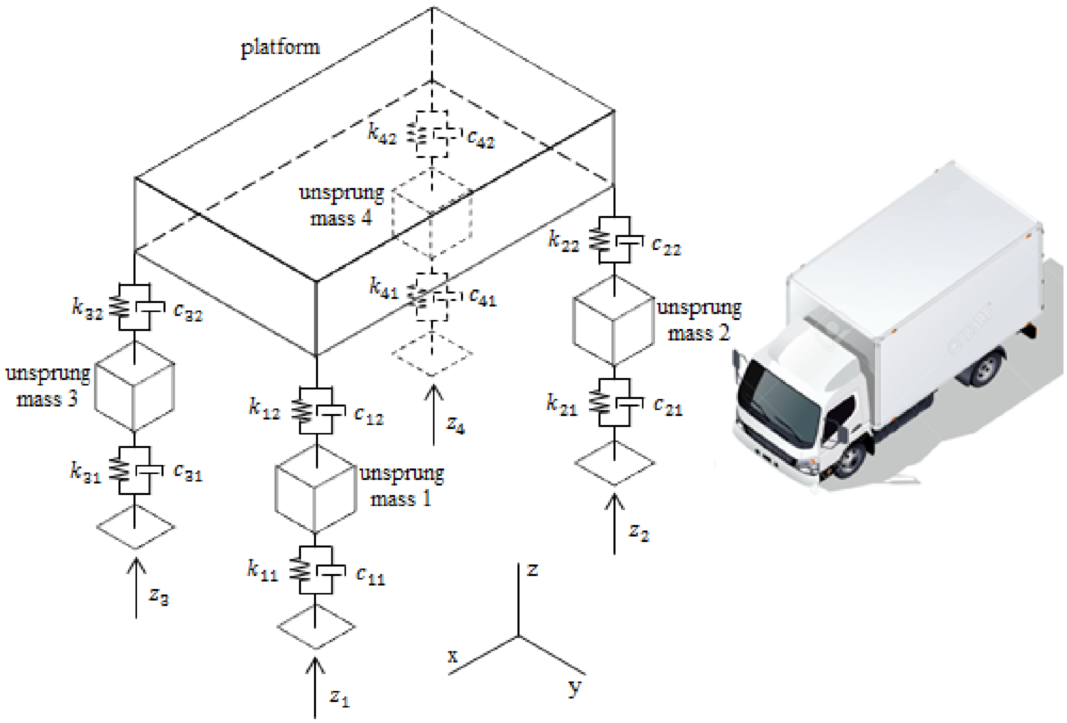

Figure 1. Physical sketch for dynamical analysis of a fully independent suspension vehicle.

In Fig. 1, each pair of spring-dashpot assembly, has a spring stiffness k_{ij} and a damping coficient c_{ij}, where "i" ($i = 1, 2, 3, 4$) denotes the specific unsprung mass, recalling that the indexes $1, 2, 3, 4$ hold for: front-left; rear-left; front-right and rear-right wheels, respectively; whereas "j" ($j = 1, 2$) denotes which pair of spring-dashpot assembly is being considered, such that $1, 2$ stand for: inferior set (tires behavior) and superior set (suspension behavior), respectively. Accordingly, $z_i(t)$ are the time-varying ground displacements imposed to each wheel, whose mathematical prescribed functions will be adressed later in the paper.

Figure 2 depicts the free-body diagram for the platform (Fig. 2a) and for the unsprung masses (Fig. 2b). In this layout, concerning the geometry of the platform, its center of mass (point G) is placed in the medium horizontal plane with longitudinal symmetry, although a little shifted frontward (due to the mass of the cabin). The lengths a_1 and a_2 have to do with the longitudinal length and help to define the point G position (notice that $a_1 + a_2$ constitutes the wheelbase of the truck); while a_3 and a_4 correspond to the width and height of the truck chassis.

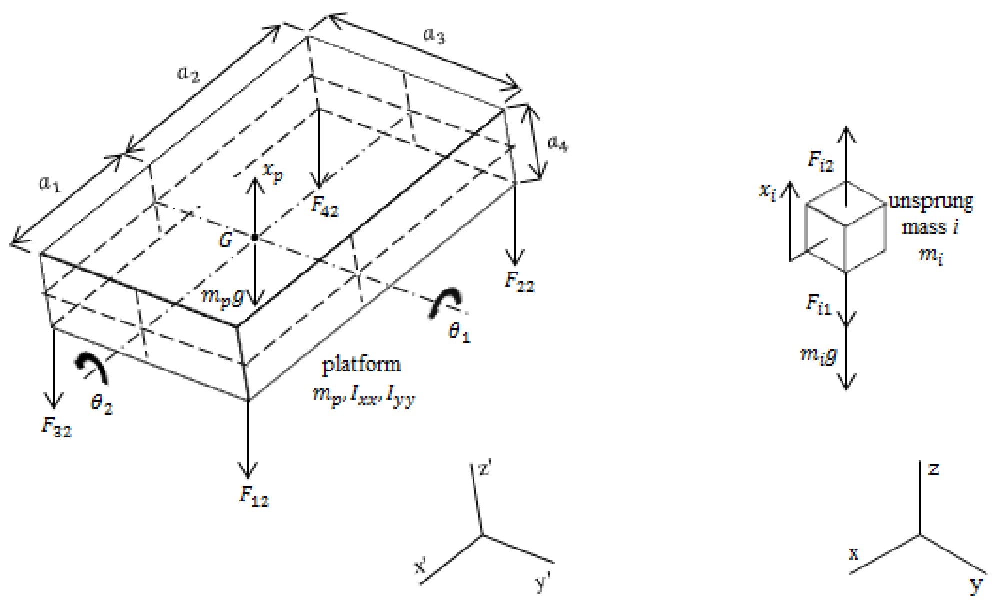

(a) (b)

Figure 2. Free-body diagram. (a) Platform; (b) Each unsprung mass.

Still concerning Fig. 2, m_p represents the mass of the platform, while I_{xx} and I_{yy} are, respectively, the principal mass moments of inertia of the platform around the axis x' and y' of the non-inertial reference frame (x', y', z') attached to the platform; g denotes the acceleration of gravity; x_p is the absolute linear displacement of the platform in the "z" direction (bounce); θ_1 and θ_2 are the absolute angular displacements in the y' (pitch) and x' (roll) directions; m_i denotes each unsprung mass of the suspension elements; x_i is the absolute linear displacement in the "z" direction of each unsprung mass and, finally, F_{ij} denotes the force developed by each pair of spring-dashpot assembly, considering the convention already defined, where: $(i = 1,2,3,4)$ and $(j = 1,2)$.

Based on the free-body diagram presented in Fig. 2, it is possible to write all equations of motion associated to the proposed dynamical system, as follows. The left side of Eq. (1) displays Newton equations (in z direction) related to the vertical translation of the four unsprung masses, while the right side of Eq. (1), for the platform, shows one Newton equation (in z direction, as well) to consider the vertical "bounce" translation of the plataform and two Euler equations to consider both the transversal "pitch" rotation (in y' direction) and the longitudinal "roll" rotation (in x' direction).

$$\text{Unsprung masses}\begin{cases}\text{Front-left:} & m_1\ddot{x}_1 + F_{11} - F_{12} + m_1 g = 0\\ \text{Rear-left:} & m_2\ddot{x}_2 + F_{21} - F_{22} + m_2 g = 0\\ \text{Front-right:} & m_3\ddot{x}_3 + F_{31} - F_{32} + m_3 g = 0\\ \text{Rear-right:} & m_4\ddot{x}_4 + F_{41} - F_{42} + m_4 g = 0\end{cases} \qquad \text{Platform}\begin{cases}\text{Bounce:} & m_p\ddot{x}_p + F_{12} + F_{22} + F_{32} + F_{42} + m_p g = 0\\ \text{Pitch:} & I_{yy}\ddot{\theta}_1 + a_2\left(F_{22}+F_{42}\right) - a_1\left(F_{12}+F_{32}\right) = 0\\ \text{Roll:} & I_{xx}\ddot{\theta}_2 + \frac{a_3}{2}\left(F_{12}+F_{22}\right) - \frac{a_3}{2}\left(F_{32}+F_{42}\right) = 0\end{cases} \tag{1}$$

In order to evaluate the forces F_{i2} acting on the four corners of the plataform, it is necessary to analyse the displacents and velocities at these corners. Observing Fig. 2, the corners' displacement expressions in their nolinear form may be written as Eqs. (2), which can be approximately linearized, under the assumption of small rotations. To obtain the respective velocities, it is enough to simply derive these displacement expressions.

$$\begin{aligned} u_1 &= x_p - a_1\sin(\theta_1) + \frac{a_3}{2}\cos(\theta_1)\sin(\theta_2) \cong x_p - a_1\theta_1 + \frac{a_3}{2}\theta_2\\ u_2 &= x_p + a_2\sin(\theta_1) + \frac{a_3}{2}\cos(\theta_1)\sin(\theta_2) \cong x_p + a_2\theta_1 + \frac{a_3}{2}\theta_2\\ u_3 &= x_p - a_1\sin(\theta_1) - \frac{a_3}{2}\cos(\theta_1)\sin(\theta_2) \cong x_p - a_1\theta_1 - \frac{a_3}{2}\theta_2\\ u_3 &= x_p + a_2\sin(\theta_1) - \frac{a_3}{2}\cos(\theta_1)\sin(\theta_2) \cong x_p + a_2\theta_1 - \frac{a_3}{2}\theta_2 \end{aligned} \tag{2}$$

Again, observing the free-body diagram of Fig. 2, the restitution and dissipative forces due to both the suspension and the tire behaviors may be identified and combined to provide the forces F_{ij}, according to Eqs. (3).

$$\begin{aligned} F_{11} &= k_{11}\left(x_1 - z_1\right) + c_{11}\left(\dot{x}_1 - \dot{z}_1\right) & F_{12} &= k_{12}\left(u_1 - x_1\right) + c_{12}\left(\dot{u}_1 - \dot{x}_1\right)\\ F_{21} &= k_{21}\left(x_2 - z_2\right) + c_{21}\left(\dot{x}_2 - \dot{z}_2\right) & F_{22} &= k_{22}\left(u_2 - x_2\right) + c_{22}\left(\dot{u}_2 - \dot{x}_2\right)\\ F_{31} &= k_{31}\left(x_3 - z_3\right) + c_{31}\left(\dot{x}_3 - \dot{z}_3\right) & F_{32} &= k_{32}\left(u_3 - x_3\right) + c_{32}\left(\dot{u}_3 - \dot{x}_3\right)\\ F_{41} &= k_{41}\left(x_4 - z_4\right) + c_{41}\left(\dot{x}_4 - \dot{z}_4\right) & F_{42} &= k_{42}\left(u_4 - x_4\right) + c_{42}\left(\dot{u}_4 - \dot{x}_4\right) \end{aligned} \tag{3}$$

Substituting Eqs. (2) and their derivatives into Eqs. (3) and, after that, incorporating the forces F_{ij} to Eqs. (1), the linearized equations of motion may be written in their final form, which can be put in a matrix/vector expression with the following general structure: $[m]\{\ddot{x}\}+[c]\{\dot{x}\}+[k]\{x\}=\{F\}$, where: $[m]$, $[c]$ and $[k]$ are inertia, damping and stiffness (symmetric) matrices; while the generalized displacement vector containing seven degrees of freedom is given by the transpose of $\{x\}^T = \{x_1 \quad x_2 \quad x_3 \quad x_4 \quad x_p \quad \theta_1 \quad \theta_2\}$, with respective derivatives: velocity $\{\dot{x}\}$ and acceleration $\{\ddot{x}\}$. At last, the vector $\{F\}$ concerns the external excitations due to the weight of both unsprung masses and platform, besides the forces transmitted by the ground displacement. Equation (4) displays the expanded inertia matrix $[m]$, stiffness matrix $[k]$ and the forcing vector $\{F\}$. For convenience, the damping matrix $[c]$ is omitted, since it is similar to the stiffness matrix, despite of considering c_{ij} instead of k_{ij}.

For the purpose of numerical implementation via fourth-order *Runge-Kutta* method, it is necessary to convert the original system consisting of seven second-order ordinary differential equations into a new set of first-order ordinary differential equations with fourteen equations.

$$[m]=\begin{bmatrix} m_1 & 0 & 0 & 0 & 0 & 0 & 0 \\ 0 & m_2 & 0 & 0 & 0 & 0 & 0 \\ 0 & 0 & m_3 & 0 & 0 & 0 & 0 \\ 0 & 0 & 0 & m_4 & 0 & 0 & 0 \\ 0 & 0 & 0 & 0 & m_p & 0 & 0 \\ 0 & 0 & 0 & 0 & 0 & I_{yy} & 0 \\ 0 & 0 & 0 & 0 & 0 & 0 & I_{xx} \end{bmatrix} \qquad \{F\}=\begin{Bmatrix} k_{11}\, z_1 + c_{11}\, \dot{z}_1 - m_1\, g \\ k_{21}\, z_2 + c_{21}\, \dot{z}_2 - m_2\, g \\ k_{31}\, z_3 + c_{31}\, \dot{z}_3 - m_3\, g \\ k_{41}\, z_4 + c_{41}\, \dot{z}_4 - m_4\, g \\ -m_p\, g \\ 0 \\ 0 \end{Bmatrix} \tag{4}$$

$$[k]=\begin{bmatrix} k_{11}+k_{12} & 0 & 0 & 0 & -k_{12} & k_{12}\,a_1 & -k_{12}\,a_3/2 \\ 0 & k_{21}+k_{22} & 0 & 0 & -k_{22} & -k_{22}\,a_2 & -k_{22}\,a_3/2 \\ 0 & 0 & k_{31}+k_{32} & 0 & -k_{32} & k_{32}\,a_1 & k_{32}\,a_3/2 \\ 0 & 0 & 0 & k_{41}+k_{42} & -k_{42} & -k_{42}\,a_2 & k_{42}\,a_3/2 \\ -k_{12} & -k_{22} & -k_{32} & -k_{42} & \begin{pmatrix} k_{12}+k_{22}+ \\ +k_{32}+k_{42} \end{pmatrix} & \begin{pmatrix} -k_{12}\,a_1+k_{22}\,a_2+ \\ -k_{32}\,a_1+k_{42}\,a_2 \end{pmatrix} & \begin{pmatrix} k_{12}+k_{22}+ \\ -k_{32}-k_{42} \end{pmatrix}\dfrac{a_3}{2} \\ k_{12}\,a_1 & -k_{22}\,a_2 & k_{32}\,a_1 & -k_{42}\,a_2 & \begin{pmatrix} -k_{12}\,a_1+k_{22}\,a_2+ \\ -k_{32}\,a_1+k_{42}\,a_2 \end{pmatrix} & \begin{pmatrix} k_{12}\,a_1^2+k_{22}\,a_2^2+ \\ +k_{32}\,a_1^2+k_{42}\,a_2^2 \end{pmatrix} & \begin{pmatrix} -k_{12}\,a_1+k_{22}\,a_2+ \\ +k_{32}\,a_1-k_{42}\,a_2 \end{pmatrix}\dfrac{a_3}{2} \\ -k_{12}\,a_3/2 & -k_{22}\,a_3/2 & k_{32}\,a_3/2 & k_{42}\,a_3/2 & \begin{pmatrix} k_{12}+k_{22}+ \\ -k_{32}-k_{42} \end{pmatrix}\dfrac{a_3}{2} & \begin{pmatrix} -k_{12}\,a_1+k_{22}\,a_2+ \\ +k_{32}\,a_1-k_{42}\,a_2 \end{pmatrix}\dfrac{a_3}{2} & \begin{pmatrix} k_{12}+k_{22}+ \\ +k_{32}+k_{42} \end{pmatrix}\dfrac{a_3^2}{2} \end{bmatrix}$$

3. NUMERICAL RESULTS

This section shows the numerical results obtained for the dynamical response of the proposed model. The parameters adopted in the simulations are related to a 4x2 commercial light truck, considering real performance curves provided by a specific manufacturer for the front and rear suspension stiffness and damping. Besides, three different pavement conditions are imposed as ground displacement.

Figure 3 shows the empirical curves for front/rear suspension stiffness and damping. Concerning the stiffness curves (Figs. 3a and 3b – front and rear, respectively), both are symmetric, with respect to tension-compression behavior.

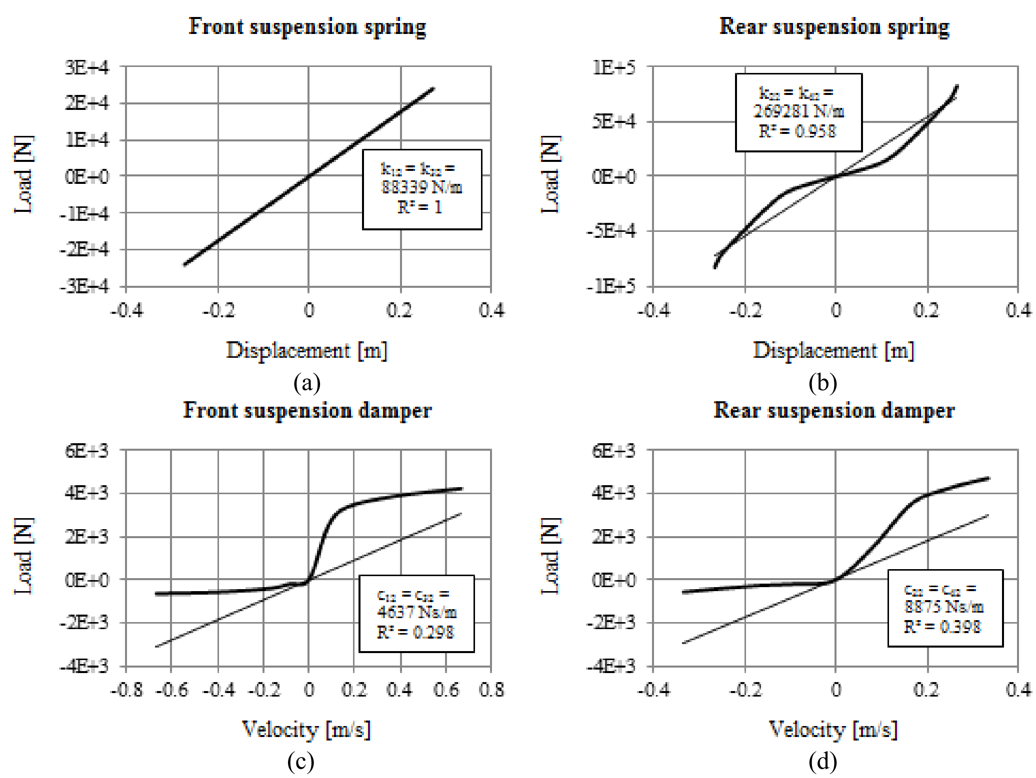

Figure 3. Empirical performance curves for front/rear suspension stiffness and damping and respective linearizations. (courtesy of MAN Latin America)

Nevertheless, the front curve presents a linear behavior, while the rear one is nonlinear. Concerning the damping curves (Figs. 3c and 3d – front and rear, respectively), both of them are nonlinear and present tension-compression asymmetry, with much larger forces under tension than under compression. The instantaneous values of the stiffness/damping coefficients are evaluated through a linear interpolation considering two subsequent values of displacement/velocity. A linear fit of these empirical curves is carried out, with the purpose of identifying equivalent constant stiffness/damping coefficients (present in the figures), in order to compare linear and nonlinear behaviors.

Figure 4 presents three different pavement conditions imposed through prescribed mathematical functions for the ground displacement on each wheel $z_i(t)$ for: $i = 1, 2, 3, 4$ denoting: front-left; rear-left; front-right and rear-right wheels, respectively. Figure 4(a) corresponds to a cobblestone road; Fig. 4(b) stands for a speed bump and Fig. 4(c) considers a hole on the road. Concerning the geometry of these obstacles, for the cobblestone: 0.1 m (width) and 0.01 m (gap between two cobblestones and groove depth); for the speed bump: 1.5 m (length) and 0.2 (height); for the hole: 1 m (length) and 0.15 (height). It is worthwhile to notice that there is a shift between the input displacements on front wheels (z_1 and z_3) and the rear ones (z_2 and z_4). This time delay is estimated based on both the vehicle wheelbase and its constant speed cruising these obstacles (30 km/h for the cobblestone; 20 km/h for the speed bump and 40 km/h for the hole). Moreover, for the specific condition of a hole on the road, only the right wheels pass through the hole.

Within this context, three analyses are of concern: the first one focuses on the comparison between linear and nonlinear suspension elements for a loaded vehicle condition submitted to a cobblestone road; the second one gives respect to the comparison between unloaded and loaded vehicle conditions considering nonlinear suspension elements submitted to a speed bump; the third one aims at the variation analyses of stiffness/damping coefficients, submitted to a hole on the road for a loaded condition.

Concerning other parameters than stiffness/damping suspension coefficients, the upcoming values are adopted, where, for some quantities, two values are presented, referring to unloaded/loaded truck condition. For the truck chassis (platform) geometry: a_1 = 1.218/2.613 m; a_2 = 2.682/1.287 m; a_3 = 1.700 m; a_4 = 2.190 m. For stiffness/damping coefficients related to the tires behavior: $k_{11} = k_{31}$ = 1e6 N/m; $k_{21} = k_{41}$ = 2e6 N/m; $c_{11} = c_{31}$ = 500 Ns/m; $c_{21} = c_{41}$ = 1000 Ns/m. For inertial quantities: m_p = 3240/9700 kg; $m_1 = m_3$ = 30 kg; $m_2 = m_4$ = 60 kg; I_{xx} = 2084/6240 kg m^2; I_{yy} = 7138/20432 kg m^2, recalling that the mass moments of inertia I_{xx} and I_{yy} are calculated by the expressions given in Eq. (5) as follows:

$$I_{xx} = \frac{1}{12} m_p \left(a_3^2 + a_4^2\right) \qquad \text{and} \qquad I_{yy} = \frac{1}{12} m_p \left[(a_1 + a_2)^2 + a_4^2\right] + m_p \left(\frac{a_2 - a_1}{2}\right)^2 \tag{5}$$

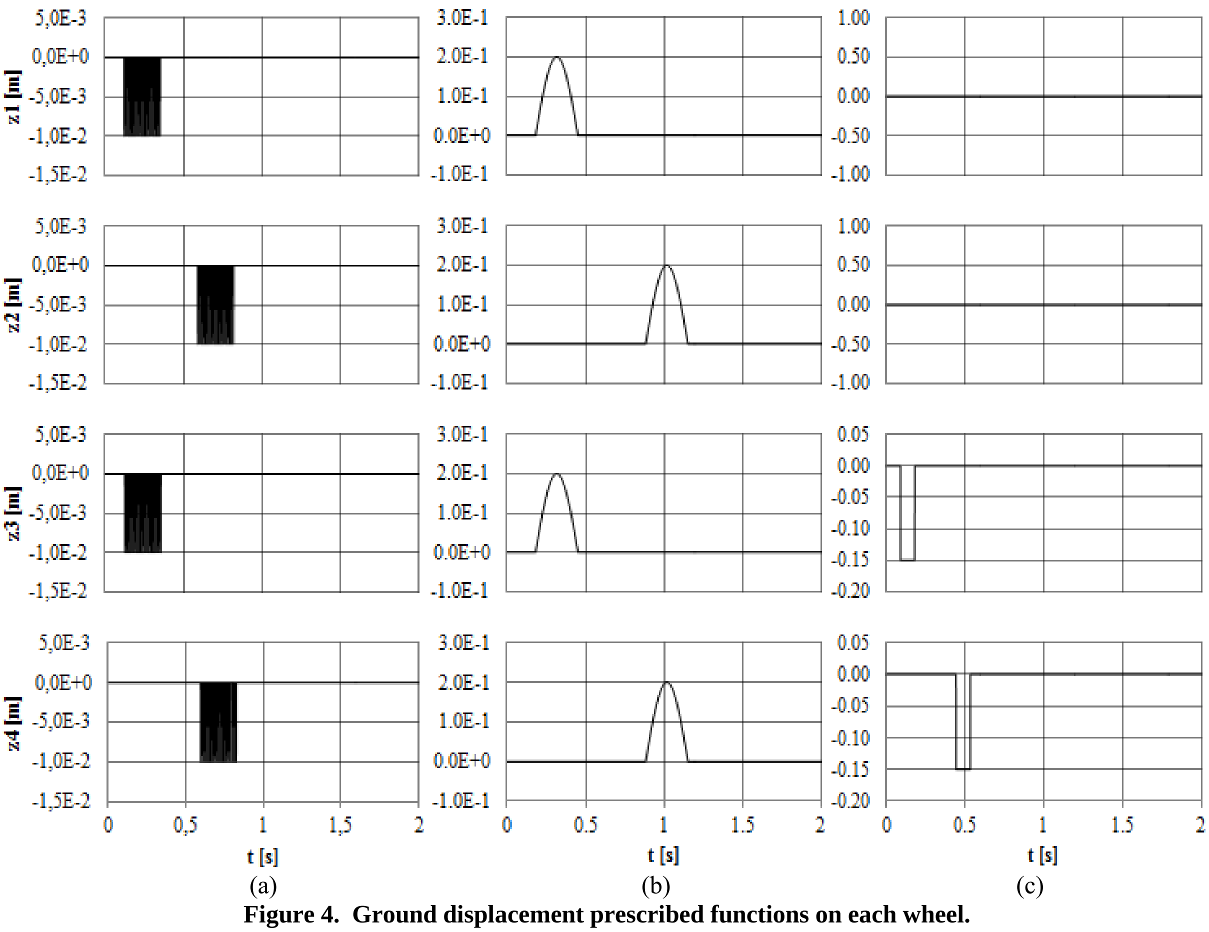

Figure 4. Ground displacement prescribed functions on each wheel.
(a) Cobblestone road; (b) Speed bump; (c) Hole on the road.

Usually, weight forces are neglected, under the assumption that they cancel out with a pre-tension in the restoring elements. Here, they are kept in the formulation, since different truck loading conditions affect both the position of the center of mass (point *G* in Fig. 2) and the pre-displacement of the chassis and unsprung masses in different ways. The value of each static pre-displacement for unloaded/loaded truck condition are respectively evaluated, as follows: $x_1 = x_3 = -0.01122/-0.01599$ m; $x_2 = x_4 = -0.00278/-0.01624$ m; $x_p = -0.09942/-0.15412$ m; $\theta_1 = 0.02916/0.01514$ rad; $\theta_2 = 0$ rad.

Figure 5 presents a displacement response comparison between linear and nonlinear suspension elements for a loaded vehicle condition submitted to a cobblestone road ground displacement.

It is noticeable the ground displacement high frequency influence over the unsprung masses displacement, besides a slight influence over the roll displacement θ_2, while bounce and pitch displacements (x_p and θ_1, respectively) are not affected. Another observation concerns the maximum/minimum amplitudes for all displacements, which are greater for the nonlinear case. According to Fig. 3(b), the higher nonlinear displacement levels induce greater forces as well. As a consequence, the nonlinear behavior of stiffness (and also for damping) of the suspension elements should be taken into account, while specifying these elements to avoid undersizing.

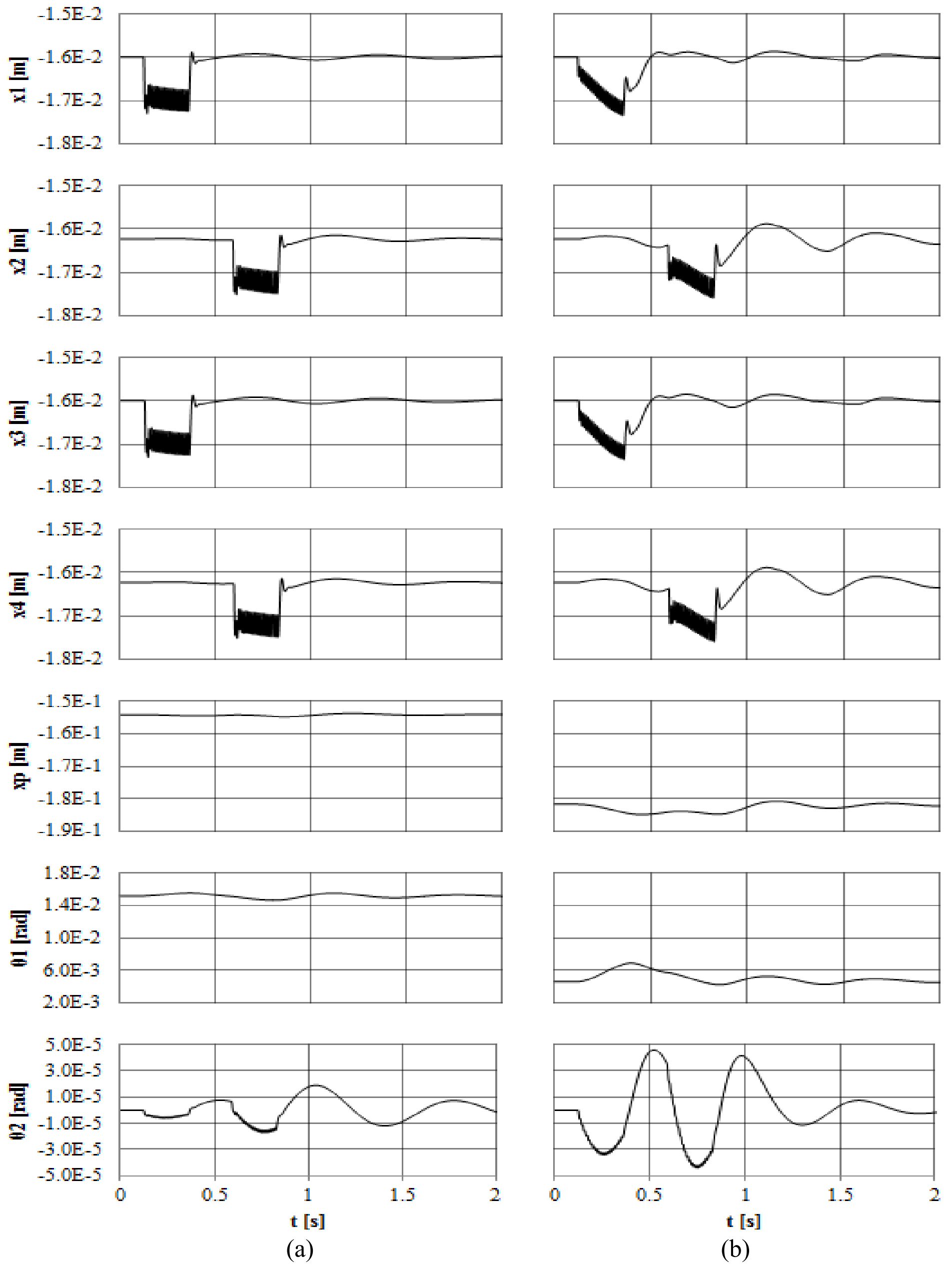

Figure 5. Displacement response comparison between linear and nonlinear suspension elements for a loaded vehicle condition submitted to a cobblestone road ground displacement. (a) Linear suspension elements; (b) Nonlinear suspension elements.

Figure 6 shows a displacement response comparison between unloaded and loaded vehicle conditions considering nonlinear suspension elements submitted to a speed bump ground displacement.

In this case, the obstacle affects equally left and right wheels, providing the same results for both sides; moreover, due to this longitudinal symmetry, roll displacement (θ_2) is null. The maximum/minimum amplitudes for all displacements are greater for the loaded case, as a consequence of higher inertial effects; therefore, inducing greater restitution/damping forces. The initial angular pitch displacement (θ_1) is greater for the unloaded condition since, for the loaded condition, the center of mass is shifted backward. Despite of that, during time evolution, there are higher amplitudes for the loaded condition.

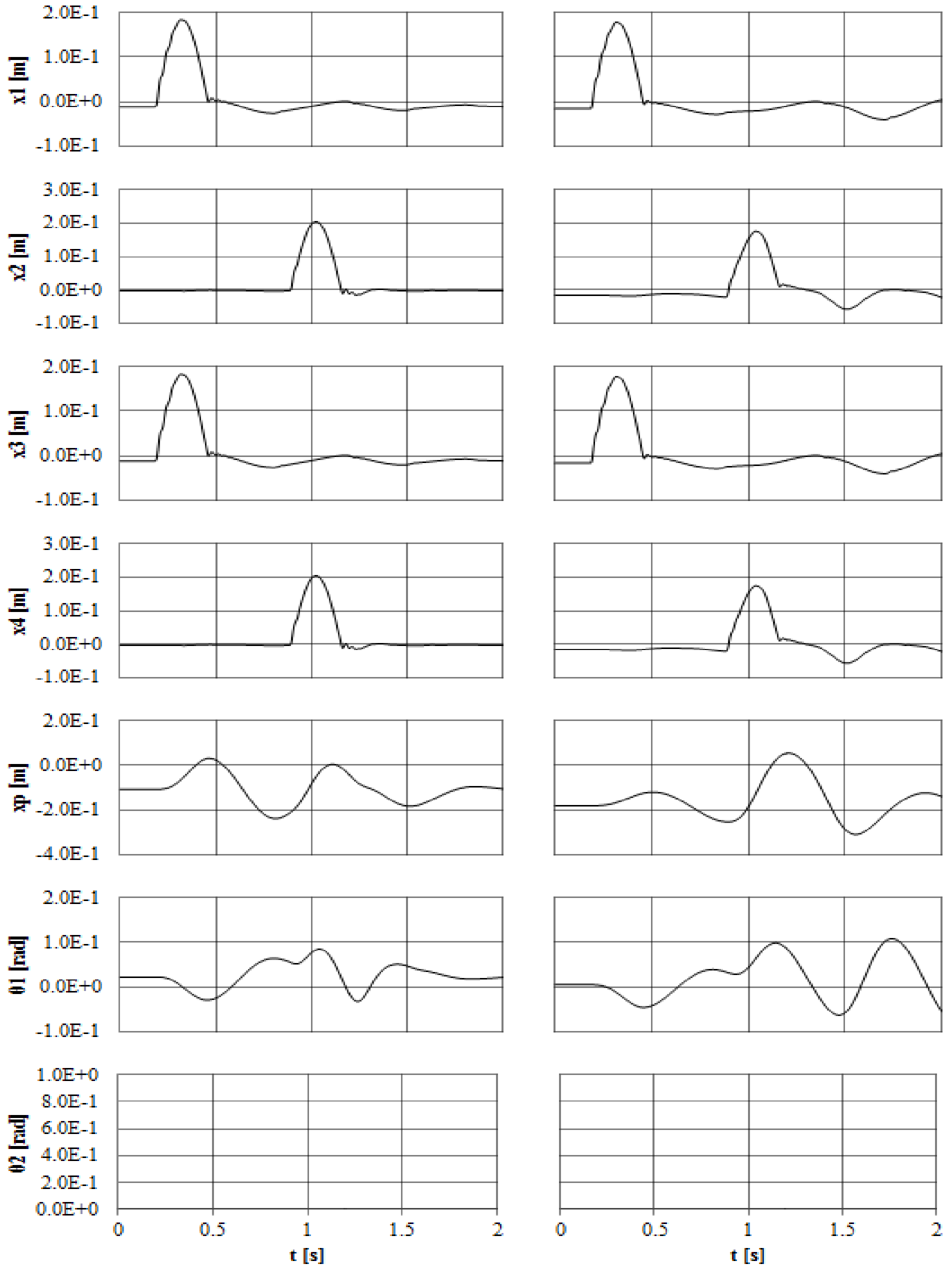

Figure 6. Displacement response comparison between unloaded and loaded vehicle conditions considering nonlinear suspension elements submitted to a speed bump ground displacement. (a) Unloaded vehicle condition; (b) Loaded vehicle condition.

Figure 7 shows the displacement responses for a loaded vehicle condition considering nonlinear suspension elements, recalling that, according to Fig. 4(c), only the right wheels are submitted to this obstacle. For the right wheels response (x_3 and x_4), there is a localized high frequency oscillation; whereas, for all other **DOF**'s, a low-frequency ongoing evanescent oscillation takes place.

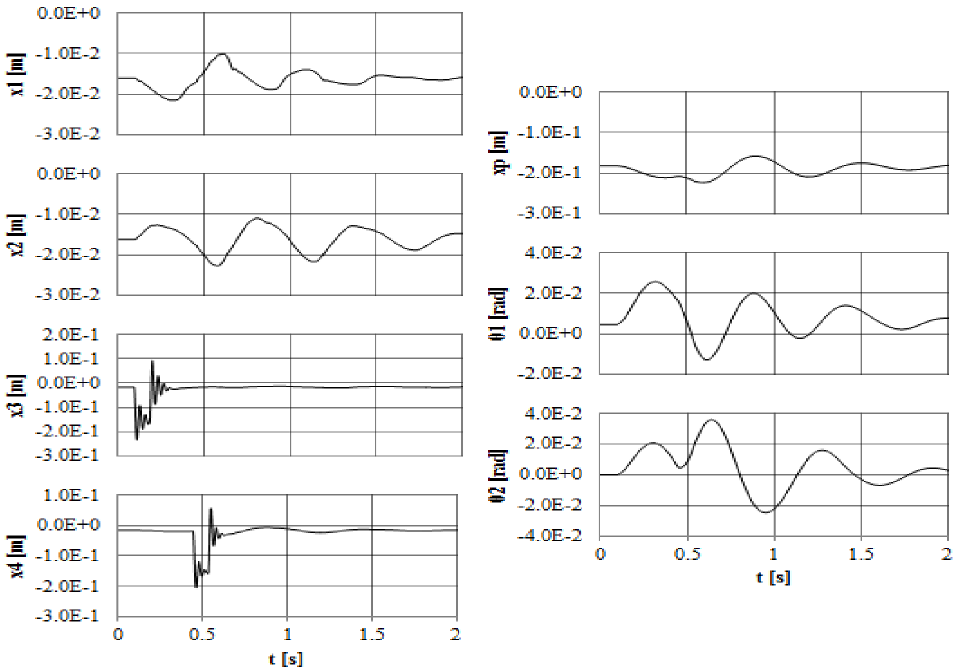

Figure 7. Displacement responses for a loaded vehicle condition considering nonlinear suspension elements submitted to a hole on the road as a ground displacement.

Considering the conditions adopted for the simulation conducted in Fig. 7 (loaded vehicle with nonlinear suspension elements submitted to a hole on the road), the next analysis considers variations in the reference performance curves for stiffness/damping suspension coefficients. To set new performance curves, the reference curves (given by Fig. 3) are multiplied by a constant factor, inducing an increase/reduction of 10, 20 and 30% in their values. Two analyses are of concern – in the first one, the stiffness curves are varied (Figs. 8a and 8b) and the front/rear damping curves assume the reference value; in the second one, the damping curves are varied (Figs. 8c and 8d) and the front/rear stiffness curves assume the reference value.

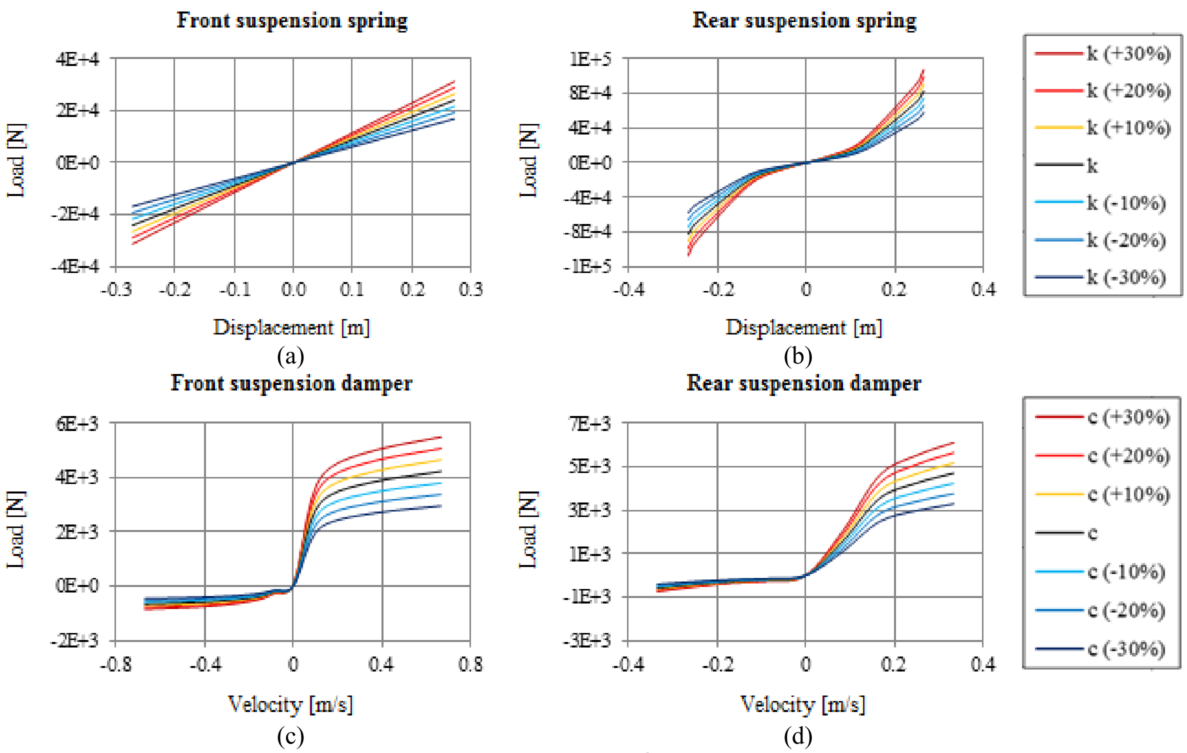

Figure 8. Empirical performance curves.
(a) Front spring stiffness variation; (b) Rear spring stiffness variation;
(c) Front damping coefficient variation; (d) Rear damping coefficient variation.

In Fig. 9, while varying the spring constants, consider the stiffness increase, which results in higher displacement amplitudes for left wheels (x_1 and x_2) and for pitch displacement (θ_1). Concerning the other four **DOF**'s, three of them (x_3, x_4 and θ_2) present a slight reduction in their amplitudes, except for the bounce displacement (x_p), which present a considerable reduction. The amplitude reduction on right wheels is due to the higher resistance presented by the "harder" springs. The bounce and roll displacements join this tendency for the same reason. The inertial effects transmission to the "harder" left springs justifies their increase. At last, the increasing pitch displacement amplitude may be attributed to asymmetric behavior between front (linear) and rear (nonlinear) springs. For stiffness reduction the analysis is analogous.

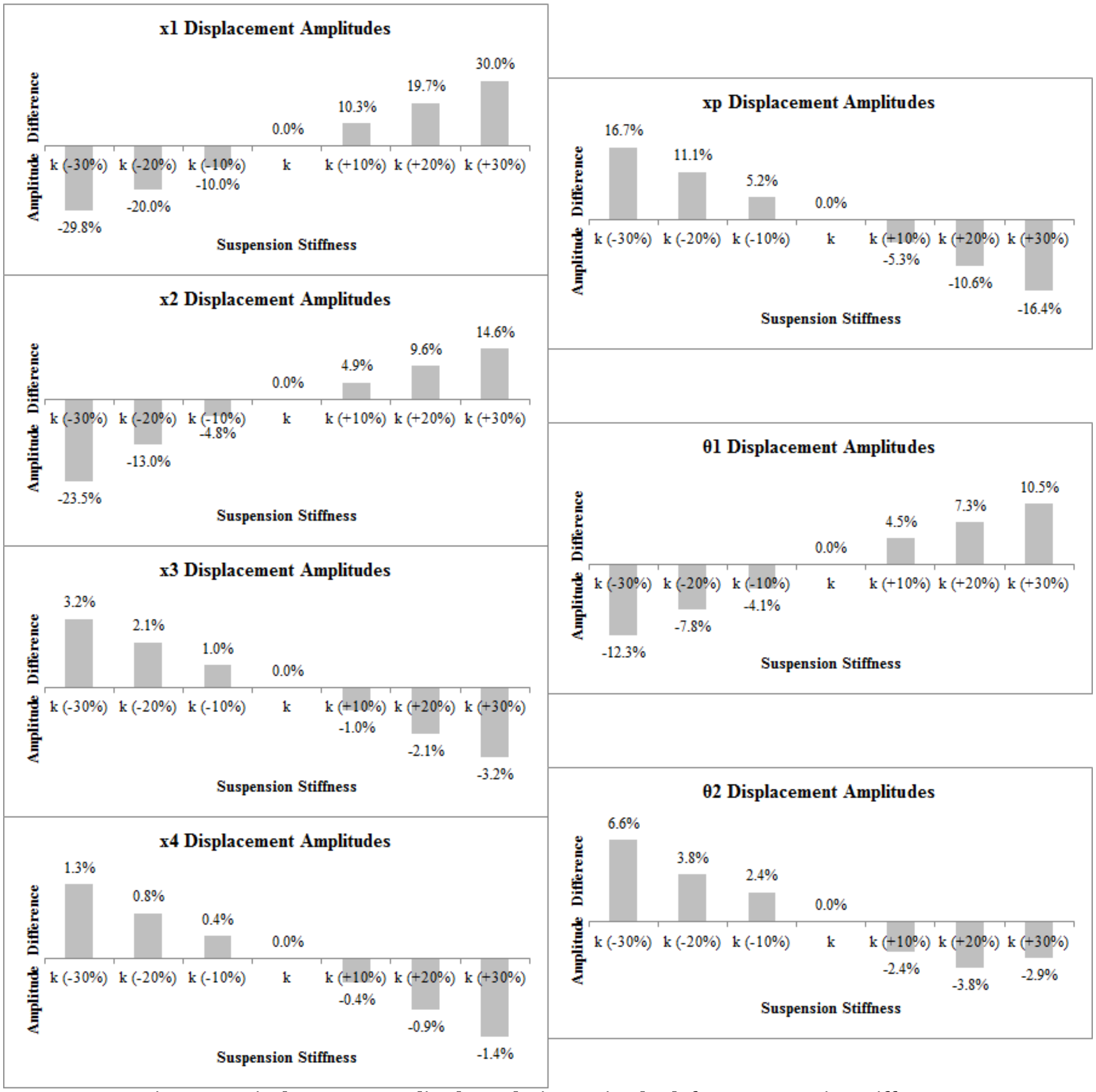

Figure 9. Displacement amplitude analysis varying both front/rear spring stiffnesses considering a hole on the road as a ground displacement.

In Fig. 10, while varying the damping coefficients, the damping increase induces lower amplitudes for all **DOF**'s, except for the front-left wheel. Obviously, with "more damping" in the system, lower amplitudes are expected. The front-left wheel higher displacement may be explained by the relevant pitch displacement reduction together with the asymmetric behavior between front (linear) and rear (nonlinear) springs. For damping reduction the analysis is analogous.

4. CONCLUDING REMARKS

This work deals with the dynamical modeling of a fully independent suspension vehicle model with seven degrees of freedom, involving bounce, pitch and roll of a rigid chassis, besides considering suspension unsprung masses and tires behavior. Besides, real nonlinear performance curves for front/rear suspension stiffness and damping are adopted. The present paper focuses on the influence of three features: different pavement conditions; nonlinear behavior of the suspension elements and load addition implications. The presented model enables an accurate description of specific response details. Moreover, it constitutes a simulation tool for other desired investigations.

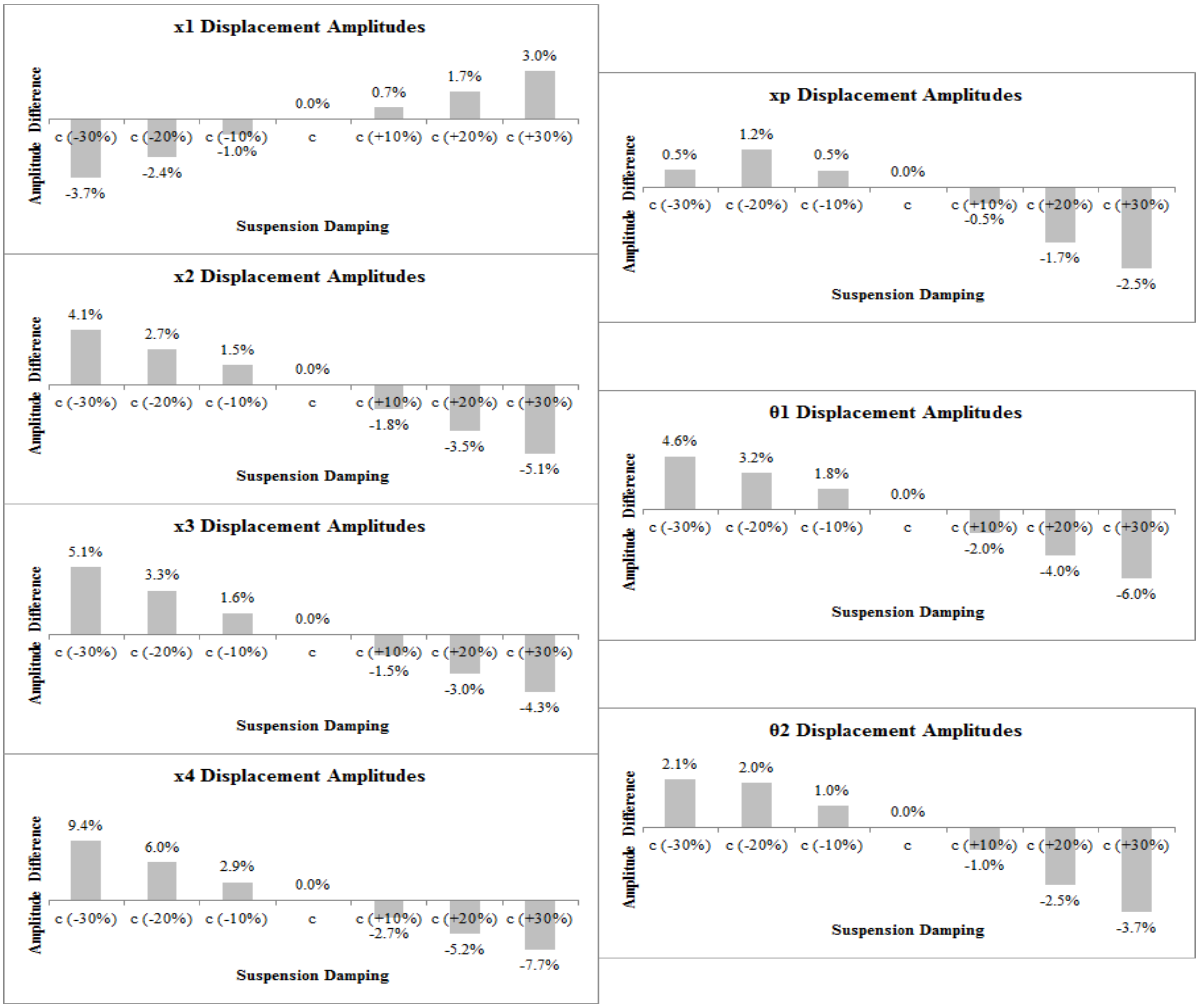

Figure 10. Displacement amplitude analysis varying both front/rear damping coefficients considering a hole on the road as a ground displacement.

5. REFERENCES

Dugard, L., Sename, O., Aubouet, S. & Talon, B.; 2012; "Full Vertical Car Observer Design Methodology for Suspension Control Applications"; Control Engineering Practice; Vol. 20; N. 9; pp. 832–845.

Gillespie, T.D.; 1992; "Fundamentals of Vehicle Dynamics"; Publisshed by SAE - Inc.; 470 pp.

Litak, G., Borowiec, M., Friswell, M.I. & Szabelski, K.; 2008 "Chaotic Vibration of a Quarter-car Model Excited by the Road Surface Profile"; Communications in Nonlinear Science & Numerical Simulation; Vol. 13; N. 7; pp. 1373–1383.

Nicolazzi, L.C., Rosa, E. & Leal, L.C.; 2001; "Uma Introdução à Modelagem Quase-estática de Veículos Automotores de Rodas"; Published by the Department of Mechanical Engineering of UFSC; 291 pp.

Rao, L.V. & Narayanan, S.; 2008; "Preview Control of Random Response of a Half-car Vehicle Model Traversing Rough Road"; Journal of Sound and Vibration; Vol. 310, N. 1–2, Pages 352–365.

Sharma, S.K., Pare, V., Chouksey, M. & Rawal, B.R.; 2016; "Numerical Studies Using Full Car Model for Combined Primary and Cabin Suspension"; Procedia Technology, Vol. 23; pp. 171–178.

Taffo, G.I. & Siewea, M.S.; 2013; "Parametric Resonance, Stability and Heteroclinic Bifurcation in a Nonlinear Oscillator with Time-delay: Application to a Quarter-car Model"; Mechanics Research Communications; Vol. 52; pp. 1–10.

Türkay, S. & Akçay, H.; 2005; "A Study of Random Vibration Characteristics of the Quarter-car Model"; Journal of Sound and Vibration; Vol. 282; N. 1–2; pp. 111–124.

Vallurupalli, S.S., Dukkipati, R.V. & Osman, M.O.; 1995; "Adaptive Active Suspension for a Half-car Model with a Stochastic Dirt Road Input"; JSAE Review; Vol. 16; pp. 367–372.

Wong, J.Y.; 2001; "Theory of Ground Vehicles"; Ed. Wiley; 4th Ed.; 592 pp.

6. ACKNOWLEDGEMENT

The authors would like to acknowledge the support of the Brazilian Research Agencies CNPq, CAPES, FAPERJ as well as INCT-EIE (National Institute of Science and Technology - Smart Structures in Engineering). The acknowledgement applies also to MAN Latin America for the supplied information.

7. RESPONSIBILITY NOTICE

The authors are the only responsible for the material included in this paper.